Mathematical Modelling and Control

http://www.aimspress.com/journal/mmc

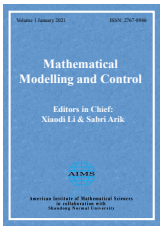

MMC, 4(1): 86–100.
DOI: 10.3934/mmc.2024008
Received: 27 August 2023
Revised: 02 December 2023
Accepted: 15 December 2023
Published: 29 March 2024

Research article

Fractional calculus analysis: investigating Drinfeld-Sokolov-Wilson system and Harry Dym equations via meshless procedures

Muhammad Nawaz Khan[1], **Imtiaz Ahmad**[2,*], **Mehnaz Shakeel**[3] **and Rashid Jan**[4,5]

[1] Mathematics in Applied Sciences and Engineering Research Group, Scientific Research Center, Al-Ayen University, Nasiriyah 64001, Iraq

[2] Institute of Informatics and Computing in Energy, Universiti Tenaga Nasional, Kajang, Selangor, Malaysia

[3] Department of Mathematics, Women University Mardan, Mardan, Pakistan

[4] Institute of Energy Infrastructure, Department of Civil Engineering, College of Engineering, Universiti Tenaga Nasional, Putrajaya Campus, Jalan IKRAM-UNITEN, Kajang 43000, Selangor, Malaysia

[5] Mathematics Research Center, Near East University North Cyprus, Mersin 99138, Turkey

* **Correspondence:** Email: imtiazkakakhil@gmail.com.

Abstract: In this study, we present two meshless schemes, namely the radial basis function (RBF) method and the polynomial method, for the numerical investigation of the time-fractional Harry Dym equation and the Drinfeld-Sokolov-Wilson system. In both methods, the temporal derivatives are estimated using the Caputo operator, while the spatial derivatives are approximated either through radial basis functions or polynomials. Additionally, a collocation approach is employed to convert the system of equations into a system of linear equations that is easier to solve. The accuracy of the methods is assessed by calculating the L_∞ error norm, and the outcomes are displayed through tables and figures. The simulation results indicate that both methods exhibit strong performance in handling the fractional partial differential equations (PDEs) under investigation.

Keywords: meshless procedures; polynomial method; RBF method; Drinfeld-Sokolov-Wilson equation; Harry Dym equation

1. Introduction

In the modern era of technology and applied sciences, numerous physical phenomena are inherently intricate. Classical calculus has traditionally been employed to mathematically model various aspects of these phenomena. However, with the rapid advancements in technology and the increasing complexity of certain physical phenomena, classical calculus may not always provide accurate models within the constraints of time and computational resources. Consequently, researchers [1–3] have redirected their focus towards fractional calculus, which proves more adept at capturing and representing the complexities of these phenomena that elude the accuracy of classical calculus. Conventional derivatives are effective for analyzing changes in a local region near a point, whereas the Caputo fractional derivative enables the analysis of changes over an interval, making it a nonlocal approach. Due to this nonlocal nature, the Caputo fractional derivative is better suited for modeling various physical phenomena, such as earthquakes, atmospheric physics, ocean climate, vibrations, dynamical systems, and polymers, etc. [4].

Significant efforts have been dedicated to the development of versatile and reliable numerical and analytical methods for solving PDEs encompassing both fractional and integer orders. These equations are of great interest in the field

of physics and engineering, such as for the fractional-order Burgers' and KdV equations [5], fractional-order anomalous solute transport model [6], fractional-order Fishers' equations in traveling waves [7], fractional-order Cauchy reaction-diffusion model [8], fractional-order option pricing models [9, 10], fraction order Sobolev equation [11], the generalized fractional-order Gardner equation being used in plasma physics to study the nonlinear propagation of ion-acoustic waves [12], multi-dimensional hyperbolic telegraph equations [13], Hirota-Satsuma coupled system [14], and others [15–20].

Here, in our present investigation, we initiate by studying the Drinfeld-Sokolov-Wilson (DSW) system involving the fractional operator of Caputo, given as follows:

$$\begin{aligned} &\frac{\partial^\beta U(x,\tau)}{\partial \tau} + 3V(x,\tau)\frac{\partial V(x,\tau)}{\partial x} = 0, \\ &\frac{\partial^\beta V(x,\tau)}{\partial \tau} + 2\frac{\partial^3 V(x,\tau)}{\partial x^3} + 2U(x,\tau)\frac{\partial V(x,\tau)}{\partial x} \\ &\qquad + V(x,\tau)\frac{\partial U(x,\tau)}{\partial x} = 0. \end{aligned} \tag{1.1}$$

Whereas $U(x,\tau)$ and $V(x,\tau)$ are unknown functions, and their fractional derivatives are denoted as $\frac{\partial^\beta U(x,\tau)}{\partial \tau}$ and $\frac{\partial^\beta V(x,\tau)}{\partial \tau}$ in the Caputo sense, and $0 < \beta \leq 1$.

When β=1, then (1.1) reduces to the standard DSW equation [21, 22]. The utilization of the fractional nonlinear DSW system as a mathematical model enables the investigation of dispersive water waves, making it a crucial component in the domain of fluid mechanics [21, 22]. Numerous numerical and analytical methodologies have been suggested by researchers to solve the Drinfeld-Sokolov-Wilson system, including the F-expansion method [23], the Homotopy analysis method [24, 25], the decomposition method [26] and the Tan method [27], etc.

The Harry Dym equation is attributed to Harry Dym by his unpublished paper, and was introduced by Kruskal and Moser [28] and the time-fractional form is given as

$$\frac{\partial^\beta U(x,\tau)}{\partial \tau} - U^3(x,\tau)\frac{\partial^3 U(x,\tau)}{\partial x^3} = 0, \quad 0 < \beta \leq 1. \tag{1.2}$$

This equation is important because it follows the conservation laws, models the system in which the dispersion is coupled with the nonlinearity, and the Painleve property does not hold in this equation. Researchers have proposed numerous numerical and analytical techniques for solving the fractional order Harry Dym equation [29, 30].

Fractional order PDEs often have complex and laborious closed form solutions, making it difficult to use existing methods to calculate them. As a result, it is often more effective to use computational techniques to approximately solve these equations. Among these techniques, meshless techniques have proven to be highly efficient and accurate in addressing a wide range of fractional and non-fractional order PDEs. There are several types of meshless methods, including the radial basis function (RBF) method, the smoothed particle hydrodynamics technique, the element-free Galerkin approach, the diffuse element method, the Fibonacci polynomials, Lucas and Fibonacci polynomials, etc.

Meshless methods are numerical techniques used to solve problems with complex geometries without relying on a fixed mesh. Every technique has its unique strengths and limitations, making it more suitable for specific problem scenarios. The meshless methods based on RBFs are a popular type that interpolate data values at scattered data points and approximate the solution of the PDE. Meshless methods are available in two variants, namely local and global approaches. Nevertheless, the global meshless method has two notable disadvantages: a dense ill-conditioned matrix and susceptibility to variations in shape parameters. Despite these challenges, RBF-based meshless methods remain popular in solving PDEs in various fields [31–34]. To address these limitations, researchers have turned to the local meshless method [35, 36]. The local RBFs meshless have a compact support around each data point, resulting in better conditioned sparse matrices. Consequently, selecting an appropriate value for the shape parameter becomes more straightforward, resulting in improved accuracy and efficiency when solving the linear equations. Unlike global methods, local RBF methods do not require the solution of dense matrices, resulting in a sparse system of linear equations that can be efficiently solved using sparse linear algebra techniques. Local RBF methods are typically more accurate and computationally efficient than global RBF methods, particularly for large-scale problems.

In recent years, researchers have utilized various

polynomial-based techniques to tackle nonlinear partial differential equations (PDEs). For instance, the authors in [37] employed B-polynomial bases to solve nonlinear PDEs. Additionally, Davari et al. [38] investigated the application of Legendre polynomials in addressing various types of PDEs (see [38–40]). The main objective of this study is to utilize two effective meshless numerical algorithms based on radial basis functions and polynomial methods to obtain an approximate solution for a nonlinear fractional-order DSW equation and Harry Dym equation. The Caputo definition is used to estimate the time fractional component, while RBF and polynomial are used to estimate the space derivatives.

The subsequent sections of this paper are structured in the following manner:

- In Sections 2 and 3, we discuss the primary objective of the study and introduce some fundamental definitions related to fractional calculus.
- Section 4 presents the proposed methodologies.
- In Section 5, we furnish numerical examples, while in Section 6, we offer our conclusions.

2. Motivation

The motivation for this article arises from the challenging nature of computing analytical solutions for nonlinear PDEs, which find applications in various scientific and engineering domains and offer valuable insights into complex physical phenomena. However, due to their nonlinear characteristics, obtaining exact solutions remains difficult. To address the challenges associated with analytical solutions, researchers have resorted to numerical methods as a feasible alternative. Numerical solutions involve dividing the problem domain into discrete elements and employing iterative algorithms to approximate the solutions at these points, proving to be efficient and practical for a wide range of problems. In this context, the article aims to present two meshless numerical schemes for the class of PDE models discussed. The first method utilizes RBFs, which are distance-dependent functions with excellent approximation capabilities. By adopting RBFs, the numerical scheme avoids the need for a structured mesh, simplifying implementation and enhancing computational efficiency. The second approach depends on polynomials as the basis for approximating solutions, offering researchers an alternative option that complements the RBF-based method. Notably, both methods exhibit a "meshless" property, eliminating the need for structured grids, thereby providing flexibility in handling complex geometries and reducing computational efforts in grid generation. The article emphasizes the high accuracy achieved by these numerical schemes, a critical aspect for reliable results in numerical simulations. The proposed methods can be designed for efficient implementation in higher dimensions, expanding their applicability to complex real-world problems involving multi-dimensional systems.

2.1. Basic definitions

Fractional derivatives are essential in fractional calculus. The following are some fundamental definitions of fractional derivatives that are commonly utilized.

Definition 2.1. *The Riemann-Liouville derivative [41, 42]*

$$\frac{\partial^\beta U(x,\tau)}{\partial \tau^\beta} = \frac{1}{\Gamma(1-\beta)} \frac{d}{d\tau} \int_\tau^T \frac{(U(x,\vartheta) - U(x,T))}{(\vartheta-\tau)^\beta} d\vartheta, \tag{2.1}$$

where $0 < \beta < 1$.

Definition 2.2. *Caputo's fractional derivative [43]*

$$\frac{\partial^\beta U(x,\tau)}{\partial \tau^\beta} = \frac{1}{\Gamma(1-\beta)} \int_0^\tau \frac{\partial U(x,\zeta)}{\partial \zeta} (\tau-\zeta)^{-\beta} d\zeta, \tag{2.2}$$

where $0 < \beta < 1$.

Definition 2.3. *The Atangana and Baleanu fractional derivative [44]*

$${}^{ABC}_{a}\frac{\partial^\beta U(x,\tau)}{\partial \tau^\beta} = \frac{B(\beta)}{1-\beta} \int_a^\tau U'(x) E_\beta\left(-\frac{\beta(\tau-x)^\beta}{1-\beta}\right) dx, \tag{2.3}$$

where $0 < \beta < 1$.

Definition 2.4. *He's fractional derivative [45]*

$$\frac{\partial^\beta U(x,\tau)}{\partial \tau^\beta} = \frac{1}{\Gamma(1-\beta)} \frac{d}{dx} \int_{\tau_0}^\tau (\tau-\zeta)^{-\beta} [U_0(\zeta) - U(\zeta)], \tag{2.4}$$

where $0 < \beta < 1$.

3. Theoretical framework for time discretization

Initially, we present the essential concepts from functional analysis that will be utilized for the discretization of the time variable.

3.1. Introduction to applied functional analysis: a preliminary overview

Let Ω be a bounded and open domain in $\mathbb{R}^2$, and let dx represent the Lebesgue measure on $\mathbb{R}^2$. For a finite value of p, the space $L^p(\Omega)$ encompasses all measurable functions U: $\Omega \longrightarrow \mathbb{R}$ that meet the condition

$$\int_\Omega |U(x)|^p dx \leq \infty.$$

This Banach space can be denoted using the norm

$$\|U\|_{L^p(\Omega)} = \left(\int_\Omega |U(x)|^p dx\right)^{\frac{1}{p}}.$$

The Hilbert space $L^p(\Omega)$ is equipped with the inner product defined as

$$(U, W) = \int_\Omega U(x)W(x)dx,$$

using the norm defined in L^2

$$\|U\|_2 = [(U, U)]^{\frac{1}{2}} = \left[\int_\Omega U(x)U(x)dx\right]^{\frac{1}{2}}.$$

Additionally, let Ω be an open domain in $\mathbb{R}^d$, where $\gamma = (\gamma_1, \ldots, \gamma_d)$ represents a d-tuple of non-negative integers, and

$$|\gamma| = \sum_{i=1}^{p} \gamma_i.$$

In accordance with this, we define the following expression:

$$D^\gamma W = \frac{\partial^{|\gamma|} W}{\partial x_1^\gamma \partial x_2^\gamma \cdots \partial x_d^\gamma}.$$

In this context, it is possible to acquire

$$\begin{aligned} H^1(\Omega) &= \left\{W \in L^2(\Omega), \frac{dW}{dx} \in L^2(\Omega)\right\}, \\ H_0^1(\Omega) &= \left\{W \in H^1(\Omega),\, W|_{\partial(\Omega)} = 0\right\}, \\ H^m(\Omega) &= \Big\{W \in L^2(\Omega), D^\gamma W \in L^2(\Omega) \\ &\qquad \text{for all positive integer } |\gamma| \leq m\Big\}. \end{aligned}$$

Here, we present the definition of an inner product within the context of a Hilbert space

$$(U, W)_m = \sum_{|\gamma|\leq m} \int_\Omega D^\gamma U(x) D^\gamma W(x) dx,$$

which gives rise to the norm

$$\|U\|_{H^m(\Omega)} = \left(\sum_{|\gamma|\leq m} \|D^\gamma U\|^2_{L^2(\Omega)}\right)^{\frac{1}{2}}.$$

The Sobolev space $X^{1,p}(I)$ is characterized as

$$X^{1,p}(I) = \left\{U \in L^p(I), \exists g \in L^P(I) : \int_I U\varphi' = \int_I g\varphi', \forall \varphi \in C^1(I)\right\}.$$

Furthermore, in this paper, we establish the definitions of the following inner product and the corresponding energy norms L^2 and H^1.

$$\|W\| = (W, W)^{1/2}, \quad \|W\|_1 = (W, W)_1^{1/2}$$

and

$$|W|_1 = \left(\frac{\partial W}{\partial x}, \frac{\partial W}{\partial x}\right)^{1/2},$$

by inner products of $L^2(\Omega)$ and $H^1(\Omega)$

$$(U, W) = \int U(x)W(x)dx, \quad (U, W)_1 = (U, W) + \left(\frac{\partial U}{\partial x}, \frac{\partial W}{\partial x}\right),$$

respectively.

Let us define $\Delta\tau = \frac{T}{M}$ as the mesh size in time, and $\tau_i = i\Delta\tau, i \in \mathbb{N}^+$, are the total M temporal discretization points.

Lemma 3.1. *Let us suppose $\eta(t) \in C^2[0, T]$ and $0 < \beta < 1$. Then, it holds that*

$$\int_0^{\tau_i} \eta'(x)\,(\tau_i - x)^{-\beta}\, dx = \sum_{p=1}^{i} \frac{\eta\left(\tau_p\right) - \eta\left(\tau_{p-1}\right)}{\Delta\tau},$$

$$\int_{\tau_{p-1}}^{\tau_p} (\tau_i - x)^{-\beta}\, dx + R^i, \quad 1 \leq i \leq M$$

and

$$\left|R^i\right| \leq \left(\frac{1}{2(1-\beta)} + \frac{1}{2}\right)\Delta\tau^{2-\beta} \max_{0\leq\tau\leq\tau_i} \left|\eta''(t)\right|.$$

Proof. See Sun et al. [46]. □

Lemma 3.2. *Let* $0 < \beta < 1$,

$$a_0 = \frac{1}{\Delta\tau\Gamma(1-\beta)}$$

and

$$b_p = \frac{\Delta\tau^{1-\beta}}{(1-\beta)}\left[(p+1)^{1-\beta} - (p)^{1-\beta}\right],$$

then,

$$\begin{aligned}&\frac{1}{\Gamma(1-\beta)}\int_0^{\tau_i}\frac{\eta'(x)}{(\tau_i - x)^{\beta}}dx\\ &- a_0\left[b_0\eta(\tau_i) - \sum_{p=1}^{i-1}\left(b_{i-p-1} - b_{i-p}\right)\eta\left(\tau_p\right) - b_{i-1}\eta(0)\right]\\ &\leq \frac{1}{2\Gamma(1-\beta)}\left(1 + \frac{1}{(1-\beta)}\right)\Delta\tau^{2-\beta}\max_{0\leq\tau\leq\tau_i}\left|\eta''(\tau)\right|.\end{aligned}$$

Proof. Directly follows from Lemma 3.1. □

Lemma 3.3. *Let*

$$b_p = \frac{\Delta\tau^{1-\beta}}{(1-\beta)}\left[(p+1)^{1-\beta} - (p)^{1-\beta}\right],$$

where $0 < \beta < 1$, $p = 0, 1, 2, \ldots$, *then* $b_0 > b_1 > b_2 > \cdots > b_p \to 0$, *as* $p \to \infty$.

Proof. See Sun et al. [46]. □

4. Formulation of the schemes

Here are the formulations for the discretization of the underlying fractional-order PDE models. In order to discretize the space derivatives appearing in Eqs (1.1) and (1.2), the following methods are used:

(1) Local meshless radial basis function method (MRBFM).

(2) Meshless polynomial method (MPM).

4.1. Local meshless radial basis function method

The problem under consideration involves the discretization of N distinct center points denoted as

$$x = \{x_1^c, x_2^c, \cdots, x_N^c\}$$

in the domain R. These centers, which can be positioned freely without any restrictions on the problem domain's structure, play a crucial role in the local RBF approach. At each of these N centers, a local interpolant of the form is considered as follows: insert the form of the local interpolant here

$$U(x,\tau) = \sum_{k\in I_i}\lambda_k\chi\left(\|x - x_k^c\|_2, \varepsilon_i\right), \tag{4.1}$$

where λ represents a vector of expansion coefficients, χ be a RBF, and I_i be the vector associated with center i, which includes the center number and the indices of its $n-1$ nearest neighboring centers. We refer to each center and its $n-1$ neighbors as a stencil.

$$U(x_k) = U_k, \quad k \in I_i, \tag{4.2}$$

and the following $n \times n$ linear systems are generated for each stencil, giving N

$$B\lambda = \mathbf{U}_1. \tag{4.3}$$

The expansion coefficients of the above linear system can be determined. The system matrix or interpolation matrix is the term referring to the matrix B. The elements of the local system matrices are

$$b_j^k = \chi\left(\|x_j^c - x_k^c\|_2, \varepsilon_i\right), \quad j,k = I_i(1), I_i(2), \cdots, I_i(n). \tag{4.4}$$

Any type of RBFs can be taken into account, but in this article our choice is the multiquadric (MQ) RBF, which is given as

$$\chi(r,\varepsilon) = \sqrt{1 + r^2\varepsilon^2}. \tag{4.5}$$

Applying a linear differential operator $\mathfrak{L}$ to Eq (4.1) and evaluating it at the center, on which the stencil is based, yields an approximation of the derivatives of a function v at the center locations

$$\mathfrak{L}U(x_i) = \sum_{k\in I_i}\lambda_k\mathfrak{L}\chi\left(\|x_i^c - x_k^c\|_2, \varepsilon_i\right). \tag{4.6}$$

The above equation, when simplified, can be expressed as follows:

$$\mathfrak{L}U(x_i) = \mathbb{K}.\lambda, \tag{4.7}$$

where λ represents the RBF expansion coefficients vector of order $n \times 1$, whereas $\mathbb{K}$ is of order $1 \times n$, consisting of the components

$$\mathbb{K}_i = \mathfrak{L}\chi\left(\|x_i^c - x_k^c\|_2, \varepsilon_i\right), \quad k \in I_i. \tag{4.8}$$

By realizing that, the coefficients of the RBF expansion can be eliminated from Eq (4.7) as

$$\mathfrak{L}U(x_i) = \mathbb{K}B^{-1}U(I_i) = (\mathbb{K}B^{-1})U(I_i) = \mathbf{W}.U(I_i), \quad (4.9)$$

where $\mathbf{W} = \mathbb{K}B^{-1}$ is the stencil weights. The function values in the stencil's center are therefore multiplied by the weights to approximate the space derivatives.

4.2. Meshless polynomial method

We select N nodes $(x_i, i = 1, 2, \cdots, N)$ within the domain $\Omega \cup \delta\Omega$, where N_a nodes are located in Ω, and N_b nodes are positioned on the boundary $\delta\Omega$ $(N = N_a + N_b)$. The approximated representation of the function $U(x, \tau)$ is denoted as $U^N(x, \tau)$. Let us consider the following:

$$U^N(x, \tau) = \sum_{i=1}^{N} \Psi_i \mathfrak{p}_i = \mathfrak{P}^T(x)\mathbf{\Psi}, \quad (4.10)$$

where $\mathfrak{P}(x, r)$ is a polynomial and

$$\mathfrak{P}(x) = [\mathfrak{p}_1(x), \mathfrak{p}_2(x), \cdots, \mathfrak{p}_N(x)]^T.$$

Let $U^N(x_i, \tau) = U_i$, then Eq (4.10) can further be written as

$$\mathbf{A\Psi} = \mathbf{U}, \quad (4.11)$$

where

$$\mathbf{U} = [U_1, U_2, \cdots, U_N]^T, \quad \mathbf{\Psi} = [a_1, a_2, \cdots, a_N]^T$$

and

$$A = \begin{bmatrix} \mathfrak{P}^T(x_1) \\ \mathfrak{P}^T(x_2) \\ \vdots \\ \mathfrak{P}^T(x_N) \end{bmatrix} = \begin{bmatrix} \mathfrak{p}_1(x_1) & \mathfrak{p}_2(x_1) & \cdots & \mathfrak{p}_N(x_1) \\ \mathfrak{p}_1(x_2) & \mathfrak{p}_2(x_2) & \cdots & \mathfrak{p}_N(x_2) \\ \vdots & \vdots & \ddots & \vdots \\ \mathfrak{p}_1(x_N) & \mathfrak{p}_2(x_N) & \cdots & \mathfrak{p}_N(x_N) \end{bmatrix}.$$

From (4.11), we have

$$\mathbf{\Psi} = \mathbf{A}^{-1}\mathbf{U}, \quad (4.12)$$

It follows from Eqs (4.10) and (4.12) that

$$U^N(x) = \mathfrak{P}^T(x)\mathbf{A}^{-1}\mathbf{U}, \quad (4.13)$$

$$U^N(x) = \mathbf{N}(x)U, \quad (4.14)$$

where

$$\mathbf{N}(x) = \mathfrak{P}^T(x)\mathbf{A}^{-1}.$$

So far, we have utilized the meshless polynomial approach to approximate the space derivative, resulting in a system of time-fractional ODEs for the underlying PDE models. Our next step is to apply the fractional operator of Caputo to solve this system of ODEs.

4.3. Temporal approximation schemes

The time derivative denoted by $\frac{\partial^\beta U(x,\tau)}{\partial \tau^\beta}$ using Caputo's method, where $0 < \beta \leq 1$, is

$$\frac{\partial^\beta U(x,\tau)}{\partial \tau^\beta} = \begin{cases} \frac{1}{\Gamma(1-\beta)} \int_0^\tau \frac{\partial U(x,\zeta)}{\partial \zeta} (\tau - \zeta)^{-\beta} d\zeta, & 0 < \beta < 1, \\ \frac{\partial U(x,\tau)}{\partial \tau}, & \beta = 1. \end{cases} \quad (4.15)$$

Taking into account $M + 1$ equidistant time points $\tau_0, \tau_1, \ldots, \tau_M$ within the interval $[0, \tau]$, where the time step is denoted by $\Delta\tau$ and $\tau_i = i\Delta\tau$ for $i = 0, 1, 2, \cdots, M$, we utilize a first-order finite difference scheme to approximate the time fractional derivative term as follows:

$$\begin{aligned} &\frac{\partial^\beta U(x, \tau_{i+1})}{\partial \tau^\beta} \\ &= \frac{1}{\Gamma(1-\beta)} \int_0^{\tau_{i+1}} \frac{\partial U(x,\zeta)}{\partial \zeta} (\tau_{i+1} - \zeta)^{-\beta} d\zeta \\ &= \frac{1}{\Gamma(1-\beta)} \sum_{p=0}^{i} \int_{p\Delta\tau}^{(p+1)\Delta\tau} \frac{\partial U\left(x,\zeta_p\right)}{\partial \zeta} \left(\tau_{p+1} - \zeta\right)^{-\beta} d\zeta. \end{aligned} \quad (4.16)$$

The approximation for $\frac{\partial U(x,\zeta_p)}{\partial \zeta}$ is given by the following expression:

$$\frac{\partial U\left(x,\zeta_p\right)}{\partial \zeta} = \frac{U\left(x,\zeta_{p+1}\right) - U\left(x,\zeta_p\right)}{\zeta} + O(\Delta\tau). \quad (4.17)$$

Next,

$$\begin{aligned} &\frac{\partial^\beta U(x, \tau_{i+1})}{\partial \tau^\beta} \\ &= \frac{1}{\Gamma(1-\beta)} \sum_{p=0}^{i} \frac{U\left(x,\tau_{p+1}\right) - U\left(x,\tau_p\right)}{\Delta\tau} \int_{p\Delta\tau}^{(p+1)\Delta\tau} \left(\tau_{p+1} - \zeta\right)^{-\beta} d\zeta \\ &= \frac{1}{\Gamma(1-\beta)} \sum_{p=0}^{i} \frac{U\left(x,\tau_{i+1-p}\right) - U\left(x,\tau_{i-p}\right)}{\Delta\tau} \int_{p\Delta\tau}^{(p+1)\Delta\tau} \left(\tau_{p+1} - \zeta\right)^{-\beta} d\zeta \\ &= \begin{cases} \frac{\Delta\tau^{-\beta}}{\Gamma(2-\beta)} \left(U^{i+1} - U^i\right) + \frac{\Delta\tau^{-\beta}}{\Gamma(2-\beta)} \sum_{p=1}^{i} \left(U^{i+1-p} - U^{i-p}\right) \left[(p+1)^{1-\beta} - p^{1-\beta}\right], & i \geq 1, \\ \frac{\Delta\tau^{-\beta}}{\Gamma(2-\beta)} \left(U^1 - U^0\right), & i = 0. \end{cases} \end{aligned}$$

Let

$$a_\beta = \frac{\Delta\tau^{-\beta}}{\Gamma(2-\beta)}$$

and

$$b_p = (p+1)^{1-\beta} - p^{1-\beta}, p = 0, 1, \cdots, i.$$

This equation can be written in a more precise manner as

$$\frac{\partial^\beta U(x,\tau_{i+1})}{\partial \tau^\beta} = \begin{cases} a_\beta\left(U^{i+1} - U^i\right) + a_\beta \sum_{p=1}^{i} b_p \left(U^{i+1-p} - U^{i-p}\right), & i \geq 1, \\ a_\beta\left(U^1 - U^0\right), & i = 0. \end{cases} \tag{4.18}$$

Utilizing Eq (4.18), the time fractional part of the underlying system of Eq (1.2) can be discretized as follows:

$$\frac{\partial^\beta U}{\partial \tau^\beta} = \begin{cases} a_\beta\left(U^{i+1} - U^i\right) + a_\beta \sum_{p=1}^{i} b_p \left(U^{i-p+1} - U^{i-p}\right), & i \geq 1, \\ a_\beta\left(U^1 - U^0\right), & i = 0. \end{cases} \tag{4.19}$$

4.4. Mathematical framework for the θ-weighted scheme

In this section, we implement the θ-weighted procedure to Eq (1.2) and take into account the time fractional derivative value from Eq (4.19), resulting in the following outcome:

$$a_\beta U^{i+1} - \theta \mathfrak{L} U^{i+1} = \begin{cases} a_\beta U^i + (1-\theta)\mathfrak{L}U^i - a_\beta \sum\limits_{p=1}^{i} b_p \left(U^{i-p+1} - U^{i-p}\right), \\ i \geq 1, \\ a_\beta U^0 + (1-\theta)\mathfrak{L}U^0, \quad i = 0. \end{cases} \tag{4.20}$$

Next, we utilize the suggested meshless method and use RBFs to interpolate $U(x, \tau^{i+1})$. Substituting the value from Eq (4.9) into Eq (4.20), we obtain the following expression

$$(a_\beta I - \theta \mathfrak{L})U^{i+1}$$
$$= \begin{cases} (a_\beta I + (1-\theta)\mathfrak{L})U^i - a_\beta \sum\limits_{p=1}^{i} b_p \left(U^{i-p+1} - U^{i-p}\right), & i \geq 1, \\ (a_\beta I + (1-\theta)\mathfrak{L})U^0, & i = 0. \end{cases}$$

We get

$$(a_\beta I - \theta L)U^{i+1}$$
$$= \begin{cases} (a_\beta I + (1-\theta)L)U^i - a_\beta \sum\limits_{p=1}^{i} b_p \left(U^{i-p+1} - U^{i-p}\right), & i \geq 1, \\ (a_\beta I + (1-\theta)L)U^0, & i = 0. \end{cases}$$

In this context, the symbol I denotes an identity matrix, while the matrix L represents the weight matrix associated with the specific differential operator $\mathfrak{L}$

$$\mathbf{U}^{i+1} = \mathbb{D}^{-1}\mathbb{E}U^i + \mathbb{D}^{-1}\mathbf{G}^{i+1}, \quad i \geq 0, \tag{4.21}$$

where

$$\mathbb{D} = a_\beta I - \theta L, \quad \mathbb{E} = a_\beta I + (1-\theta)L$$

and

$$\mathbf{G}^{i+1} = \mathbf{G}_1^{i+1} + \mathbf{G}_2^{i+1}, \quad i \geq 0.$$

Here,

$$\mathbf{G}_1^{i+1} = \left(g_1^{i+1}, 0, \cdots, g_2^{i+1}\right)$$

and

$$\mathbf{G}_2^{i+1} = -a_\beta \sum_{k=1}^{i} b_k \left(U^{i-k+1} - U^{i-k}\right),$$

whereas g_1^{i+1} and g_2^{i+1} represent specific known functions provided in the boundary conditions. Equation (4.21) enables us to compute the solution at any given time level τ^i.

4.5. Theoretical foundations of stability and convergence

The approach described by (4.21) represents a recurrence relation used to compute the solution values at time τ^{i+1} based on the solution at time τ^i. The matrix $\mathbf{M} = \mathbb{D}^{-1}\mathbb{E}$ is referred to as the amplification matrix, and its elements rely on the constant $\kappa = \frac{\Delta\tau}{h^\varsigma}$, where h represents the distance between consecutive nodes, $\Delta\tau$ denotes the time step, and ς corresponds to the order of the spatial differential operator. Let the exact solution of Eq (1.2) be u^i at time τ^i.

Theorem 4.1. *[47] Let $\Omega \subseteq \mathbb{R}^r$ be an open and bounded set that satisfies an interior cone condition. Assume that $\Phi \in C^{2k}(\Omega \times \Omega)$ of order m on $\mathbb{R}^r$ is a symmetric and strictly conditionally positive definite function. Let χ be the $(m-1)$-unisolvent set, and consider the interpolant P_f of the function $f \in \mathcal{N}_\phi(\Omega)$ over χ. Take $\beta \in \mathbb{N}_0^r$ with $|\beta| \leq k$. Then, there exist positive constants C and h_0 (independent of x, f, and Φ) such that*

$$|D^\beta f(x) - D^\beta P_f(x)| \leq C h_{\chi,\Omega}^{k-|\beta|} \sqrt{C_\Phi(x)} |f_{\mathcal{N}_\phi(\Omega)}|$$

provided that $h_{\chi,\Omega} \leq h_0$. Here,

$$C_\Phi(x) = \max_{\substack{\beta,\gamma \in \mathbb{N}_0^r \\ |\beta|+|\gamma|=2k}} \max_{w,y \in \Omega \cap B(x, c_2 h_\chi, \Omega)} |D_1^\beta D_2^\gamma \Phi(w,y)|.$$

Proof. See [47]. □

Utilizing Theorem 4.1 on infinitely differentiable functions, such as the Gaussian or MQ functions, results in achieving arbitrarily rapid algebraic convergence rates. In

other words, it holds for any natural number k and $|\beta| \leq k$ that

$$|D^{\beta} f(x) - D^{\beta} P_f(x)| \leq C_k h^{k-|\beta|} |u_{\mathcal{N}_{\phi}(\Omega)}|. \tag{4.22}$$

Whenever a function f belongs to the native space $\mathcal{N}\phi(\Omega)$, where $\mathcal{N}\phi(\Omega)$ denotes the native space of RBFs, extensive research has been conducted to explore the relationship between the constant C_k and the index k [48]. In this study, the MQ RBF is utilized, leading to the following conclusion:

$$|D^{\beta} U(x) - D^{\beta} u(x)| \leq C_k h^{k-|\beta|} |U_{\mathcal{N}_{\phi}(\Omega)}|.$$

Assuming that the scheme (4.21) exhibits spatial accuracy up to the q^{th} order, then

$$u^{i+1} = \mathbf{M} u^{i} + \mathbb{D}^{-1} \mathbf{G}^{i+1} + o((\Delta\tau)^{2-\beta} + h^{q}), \quad \Delta\tau, h \to 0. \tag{4.23}$$

Let us define the residual as $\epsilon^{i} = u^{i} - U^{i}$. Afterward,

$$\epsilon^{i+1} = \mathbf{M}\epsilon^{i} + O((\Delta\tau)^{2-\beta} + h^{q}), \quad \Delta\tau, h \to 0. \tag{4.24}$$

The stability of scheme (4.21) is ensured by adhering to Lax-Richtmyer's condition [49]:

$$\|\mathbf{M}\| \leq 1. \tag{4.25}$$

When the vector $\mathbf{M}$ follows a normal distribution, its norm $\|\mathbf{M}\|$ is equal to $\beta(\mathbf{M})$. Otherwise, for all cases, the inequality $\beta(\mathbf{M}) \leq \|\mathbf{M}\|$ holds true, provided that the step size h is chosen to be sufficiently small, and the result as well as the initial conditions of the given problem are suitably smooth. In order to maintain a constant value of $\kappa = \frac{\Delta\tau}{h^{q}}$, we take the limit $\Delta\tau \to 0$. Consequently, a constant C exists, such that

$$\|\epsilon^{i+1}\| \leq \|\mathbf{M}\| \|\epsilon^{i}\| + C((\Delta\tau)^{2-\beta} + h^{q}), \tag{4.26}$$

where $i = 0, 1, 2, \cdots, T \times M$. Given that the residual ϵ^{i} fulfills zero initial and boundary conditions, it follows that $\epsilon^{0} = 0$. Thus, employing mathematical induction,

$$\|\epsilon^{i+1}\| \leq \left(1 + \|\mathbf{M}\|^{2} + \|\mathbf{M}\|^{3} + \cdots + \|\mathbf{M}\|^{i-1}\right) C((\Delta\tau)^{2-\beta} + h^{q}), \tag{4.27}$$

where $i = 0, 1, 2, \cdots, T \times M$, using the condition given in Eq (4.25),

$$\|\epsilon^{i+1}\| \leq iC((\Delta\tau)^{2-\beta} + h^{q}), \tag{4.28}$$

where $i = 0, 1, 2, \cdots, T \times M$. Hence, the scheme is convergent.

5. Results and discussions

The primary objective of this section is to conduct a comprehensive evaluation of the effectiveness of the two suggested numerical methods by subjecting them to rigorous testing on a carefully chosen test problems. To quantitatively assess the performance and efficiency of these computational approaches, we employ the absolute error (L_{abs}) and maximum error (L_{∞}) norms. Subsequently, we compare the computed results with exact solutions and results obtained through a previously established method. This comparative analysis allows us to gain valuable insights into the accuracy and reliability of the proposed methods in solving the targeted PDEs.

Test problem 5.1. *Let us examine the test problem associated with the coupled Drinfeld's-Sokolov-Wilson system* (1.1)*. The analytical solution for this problem has been documented in [26]:*

$$U(x,\tau) = \frac{(\beta - 4k)}{2} + 3k^{2} sech^{2}(k(x - \beta\tau)), \quad 0 < \beta \leq 1,$$
$$V(x,\tau) = 2k\sqrt{\frac{\beta}{2}} sech(k(x - \beta\tau)), \quad 0 < \beta \leq 1. \tag{5.1}$$

Tables 1 and 2 display the numerical outcomes of the proposed methods for the coupled Drinfeld's-Sokolov-Wilson system in test problem 5.1. These results are obtained by varying the final time τ and the spatial point x. Upon analyzing these tables, it becomes apparent that both suggested methods yield highly favorable results. However, when comparing the results of the two methods, it becomes apparent that the MPM method demonstrates higher accuracy and consistency in solving this particular test problem.

Tables 3 and 4 present the numerical results of the suggested approaches for the coupled Drinfeld's-Sokolov-Wilson system in test problem 5.1. These results are obtained by varying the final time τ and the fractional-order β. Upon examining these tables, it becomes clear that both suggested approaches yield highly favorable results. Nevertheless, when comparing the results of the two methods, it becomes apparent that the MPM method demonstrates higher accuracy and consistency in solving this particular test problem.

Table 1. Comparison of L_∞ of U at $\beta = 1$ for test problem 5.1.

τ	$x = 0.5$		$x = 1$		$x = 2$		$x = 3$	
	MRBFM	MPM	MRBFM	MPM	MRBFM	MPM	MRBFM	MPM
0.1	6.1617e−15	6.6613e−16	6.1617e−15	7.7716e−16	5.6066e−15	6.6613e−16	7.6605e−15	6.6613e−16
0.2	1.7208e−15	1.6098e−15	1.7208e−15	1.7208e−15	1.6653e−15	1.8874e−15	1.7764e−15	1.5543e−15
0.3	2.9976e−15	2.8866e−15	3.0531e−15	3.1641e−15	2.9976e−15	3.3862e−15	3.0531e−15	2.8311e−15
0.4	4.5519e−15	4.2744e−15	4.6074e−15	4.7184e−15	4.4964e−15	5.2736e−15	4.6074e−15	4.6074e−15
0.5	6.4948e−15	5.9397e−15	6.3838e−15	6.7724e−15	6.3838e−15	8.1046e−15	6.4948e−15	6.9389e−15

Table 2. Comparison of L_∞ of V at $\beta = 1$ for test problem 5.1.

τ	$x = 0.5$		$x = 1$		$x = 2$		$x = 3$	
	MRBFM	MPM	MRBFM	MPM	MRBFM	MPM	MRBFM	MPM
0.1	1.1816e−12	7.6246e−14	9.0362e−13	3.6701e−13	1.6842e−13	9.6924e−13	1.6053e−13	1.6178e−12
0.2	1.0962e−13	1.3940e−14	7.5839e−13	6.1107e−13	2.0559e−12	1.8935e−12	3.3535e−12	3.3736e−12
0.3	2.9756e−14	1.9723e−13	9.4340e−13	7.2076e−13	2.8897e−12	2.7668e−12	4.8360e−12	5.2838e−12
0.4	2.9859e−13	5.6977e−13	9.9896e−13	6.8269e−13	3.5940e−12	3.5823e−12	6.1890e−12	7.3692e−12
0.5	6.9688e−13	1.1187e−12	9.2505e−13	4.8111e−13	4.1689e−12	4.3328e−12	7.4112e−12	9.6545e−12

Table 3. Comparison of L_∞ of U at various β for test problem 5.1.

τ	$\beta = 1$		$\beta = 0.7$		$\beta = 0.5$		$\beta = 0.3$	
	MRBFM	MPM	MRBFM	MPM	MRBFM	MPM	MRBFM	MPM
0.1	2.1094e−15	8.3267e−16	3.3192e−12	2.9013e−12	8.5691e−12	6.4824e−12	1.6253e−11	1.0634e−11
0.2	9.2704e−15	1.9429e−15	5.9859e−12	3.8821e−12	9.6629e−12	7.6106e−12	1.6077e−11	9.3403e−12
0.3	1.9929e−14	3.4417e−15	9.1961e−12	4.3178e−12	9.1155e−12	7.4878e−12	1.4242e−11	2.3388e−11
0.4	3.2307e−14	4.8295e−15	1.2987e−11	5.0992e−12	7.7701e−12	9.9465e−12	1.1701e−11	1.6082e−11
0.5	4.5020e−14	6.8279e−15	1.7311e−11	5.2339e−12	6.8103e−12	9.8176e−12	8.7930e−11	1.4962e−11

Table 4. Comparison of L_∞ of V at various β for test problem 5.1.

τ	$\beta = 1$		$\beta = 0.7$		$\beta = 0.5$		$\beta = 0.3$	
	MRBFM	MPM	MRBFM	MPM	MRBFM	MPM	MRBFM	MPM
0.1	2.9027e−12	2.2680e−12	2.6299e−10	8.9987e−10	1.0491e−09	2.7107e−09	2.1747e−09	1.0304e−08
0.2	6.6807e−12	4.9894e−12	7.0408e−10	1.4978e−09	1.0086e−09	4.5815e−09	1.9481e−09	1.9269e−08
0.3	1.0934e−11	8.2276e−12	1.2168e−09	2.0745e−09	9.1155e−10	6.5397e−09	1.4840e−09	3.0716e−08
0.4	1.5220e−11	8.9805e−12	1.7746e−09	1.2767e−09	3.5425e−10	2.5669e−09	9.2171e−10	4.2777e−09
0.5	1.9212e−11	1.1469e−11	2.3613e−09	1.3290e−09	2.7219e−10	2.5714e−09	3.7957e−10	4.0312e−09

Figures 1 and 2 depict the L_{abs} error norm for both the MRBFM and MPM, considering a fractional-order $\beta = 0.7$.

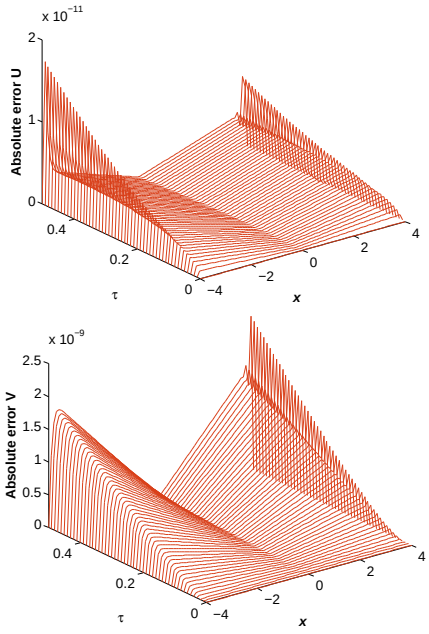

Figure 1. Absolute error of U and V using MRBFM when $\beta = 0.7$ and $N = 81$ for test problem 5.1.

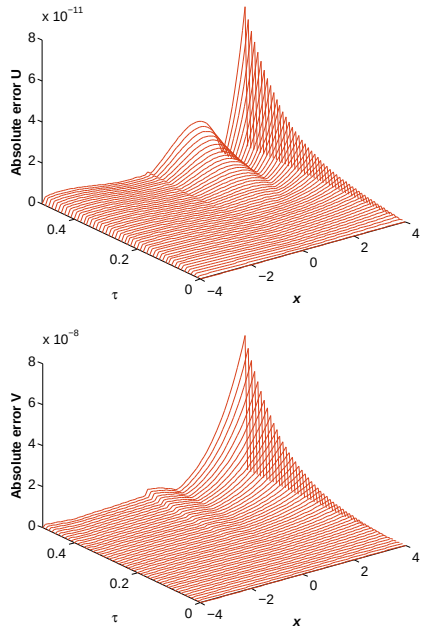

Figure 2. Absolute error of U and V using MPM when $\beta = 0.7$ and $N = 81$ for test problem 5.1.

Test problem 5.2. *Consider the test problem related to the Harry Dym equation* (1.2) *with* $\beta = 1$. *The analytical solution for this specific problem has been previously documented in [50]:*

$$U(x,\tau) = (a - \frac{3\sqrt{b}}{2}(x + b\tau)). \tag{5.2}$$

Table 5 presents the numerical results of the suggested techniques, which are compared with both the exact solution and the method described in [51], for test problem 5.2. Moreover, Table 6 demonstrates the comparison between the proposed methods and [52] for various values of β. Both tables serve as clear evidence of the superior performance of the proposed methods when compared to the methods presented in [51, 52].

Table 5. Evaluating the numerical results for $\beta = 1$ for test problem 5.2.

x	Exact	MRBFM	MPM	[51]
0.1	2.4500	2.4565	2.4472	2.4301
0.2	2.3857	2.3922	2.3837	2.3387
0.3	2.3205	2.3271	2.3193	2.2458
0.4	2.2544	2.2611	2.2539	2.1579
0.5	2.1873	2.1941	2.1875	2.0800
0.6	2.1191	2.1261	2.1201	2.0139
0.7	2.0499	2.0569	2.0515	1.9589
0.8	1.9794	1.9866	1.9817	1.9127
0.9	1.9077	1.9150	1.9106	1.8721

Additionally, Figure 3 illustrates the MRBFM results for various time values τ.

Comparisons between numerical solutions obtained using MRBFM and MPM, along with the exact solution, are depicted in Figures 4 and 5 as well. These figures also include the L_{abs} error norm. Both methods demonstrate commendable accuracy, although MPM exhibits greater accuracy compared to MRBFM. Furthermore, Figure 6 illustrates the outcomes obtained at various time points, while Figure 7 displays the comparison between exact and numerical results.

Table 6. Evaluating the numerical results for different value of β for test problem 5.2.

		$\beta = 0.25$			$\beta = 0.5$			$\beta = 1$			
x	τ	MRBFM	MPM	[52]	MRBFM	MPM	[52]	MRBFM	MPM	[52]	Exact
0	0.002	2.5198	2.3267	1.95389	2.5198	2.4805	2.46318	2.5198	2.5179	2.51858	2.51858
	0.004	2.5198	2.2902	1.83767	2.5198	2.4642	2.43951	2.5198	2.5159	2.51732	2.51732
	0.006	2.5198	2.2657	1.75768	2.5198	2.4516	2.42128	2.5198	2.5139	2.51606	2.51606
	0.008	2.5198	2.2468	1.69455	2.5198	2.4411	2.40585	2.5198	2.5119	2.5148	2.5148
0.3	0.002	2.3271	2.1750	1.73291	2.3271	2.2961	2.26811	2.3271	2.3256	2.26811	2.32581
	0.004	2.3271	2.1462	1.60916	2.3271	2.2833	2.24345	2.3271	2.3240	2.3245	2.3245
	0.006	2.3271	2.1270	1.52351	2.3271	2.2734	2.22443	2.3271	2.3224	2.32319	2.32319
	0.008	2.3271	2.1120	1.45563	2.3271	2.2651	2.20833	2.3271	2.3209	2.32187	2.32187
0.6	0.002	2.1261	2.0101	1.49682	2.1261	2.1024	2.06426	2.1261	2.1249	2.12468	2.12468
	0.004	2.1261	1.9881	1.36313	2.1261	2.0926	2.03839	2.1261	2.1237	2.12331	2.12331
	0.006	2.1261	1.9734	1.26987	2.1261	2.0851	2.01843	2.1261	2.1225	2.12194	2.12194
	0.008	2.1261	1.9620	1.19547	2.1261	2.0788	2.00153	2.1261	2.1213	2.12056	2.12056
1	0.002	1.8420	1.7666	1.14899	1.8420	1.8266	1.77551	1.8420	1.8412	1.84054	1.84054
	0.004	1.8420	1.7523	0.99516	1.8420	1.8203	1.7476	1.8420	1.8405	1.83907	1.83907
	0.006	1.8420	1.7427	0.88579	1.8420	1.8154	1.72602	1.8420	1.8397	1.83759	1.83759
	0.008	1.8420	1.7353	0.79719	1.8420	1.8113	1.70773	1.8420	1.8389	1.83612	1.83612

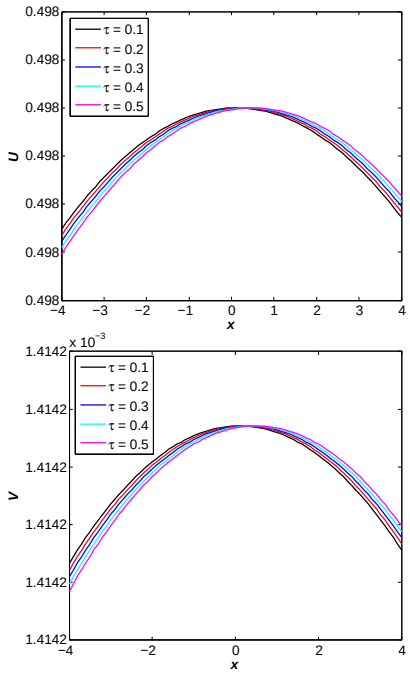

Figure 3. Numerical solution of U and V at various times using MRBFM when $\beta = 1$ and $N = 81$ for test problem 5.1.

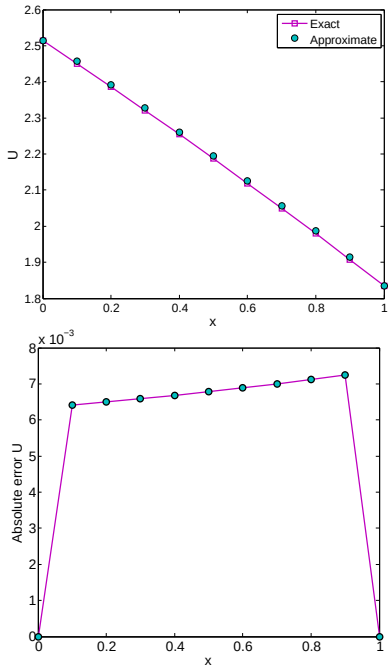

Figure 4. Exact versus approximate solutions and absolute error using MRBFM for test problem 5.2.

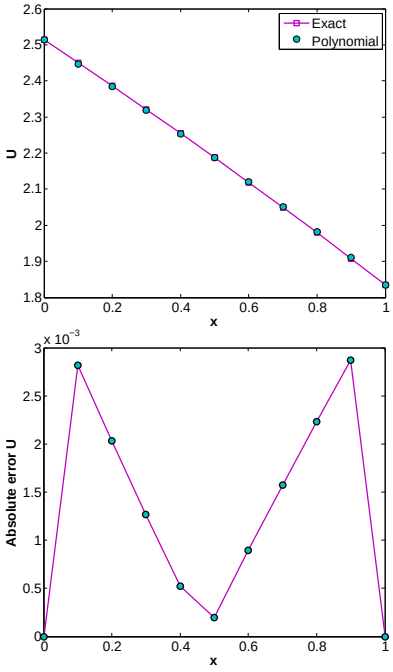

Figure 5. Exact versus approximate solutions and absolute error using polynomial method for test problem 5.2.

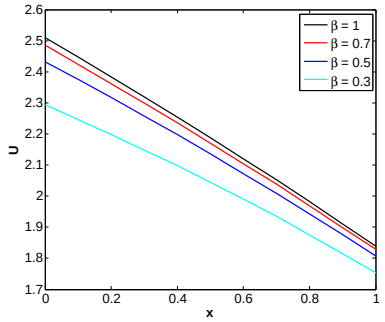

Figure 6. Approximate solutions for different values of β using polynomial method for test problem 5.2.

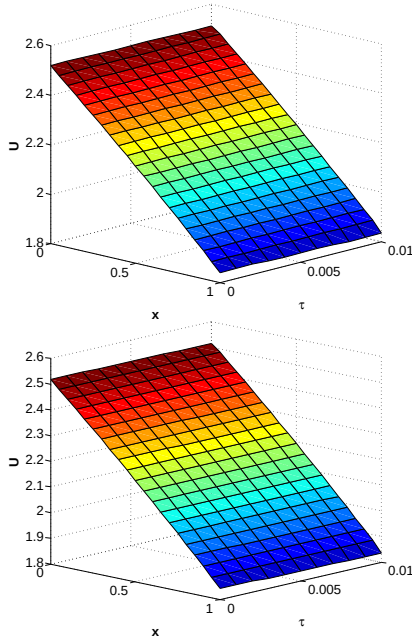

Figure 7. 3D view of approximate solutions using MRBFM and polynomial methods for test problem 5.2.

6. Conclusions

In this study, we have implemented two numerical methods, namely the meshless radial basis function method and the meshless polynomial method, to solve the time-fractional Harry Dym equation and Drinfeld-Sokolov-Wilson system. We have successfully solved two test problems through the proposed approaches. A critical aspect of our investigation involved conducting a comprehensive comparison between the computed solutions obtained from our suggested methods, exact solutions, and other methods provided in [51,52], as illustrated in the tables. The results of this comparative analysis have unequivocally demonstrated that the meshless radial basis function method and the meshless polynomial method offer better accuracy in solving these particular PDEs.

Additionally, when comparing the two suggested methods, we have observed that the results obtained from the MPM are better than those from the MRBFM. This observation strengthens the case for adopting the MPM as a preferred numerical tool for similar types of problems in the future. The graphical representations and tabulated data derived from our computations provide further compelling evidence of the effectiveness and suitability of our proposed schemes in tackling these types of PDEs. The excellent agreement between the computed solutions and the exact solutions highlights the robustness and reliability of the MRBFM and MPM in addressing fractional-order problems. In the future, this strategy can be extended to tackle higher dimensional, more complex, and challenging multi-term fractional-order problems.

Use of AI tools declaration

The authors declare they have not used artifiial intelligence tools in the creation of this article.

Conflict of interest

Authors declare no conflicts of interest in this paper.

References

1. J. Li, I. Ahmad, H. Ahmad, D. Shah, Y. Chu, Numerical solution of two-term time-fractional PDE models arising in mathematical physics using local meshless method, *Open Phys.*, **18** (2020), 1063–1072. https://doi.org/10.1515/phys-2020-0222
2. V. E. Tarasov, *Fractional dynamics: applications of fractional calculus to dynamics of particles, fields and media*, Springer Science & Business Media, 2011. https://doi.org/10.1007/978-3-642-14003-7

3. R. Caponetto, Fractional order systems, *World Sci. Ser. Nonlinear Sci. Ser. A*, **72** (2010), 1–32. https://doi.org/10.1142/9789814304207_0001
4. I. Podlubny, *Fractional differential equations*, Academic Press, 1999.
5. I. Ahmad, H. Ahmad, M. Inc, H. Rezazadeh, M. A. Akbar, M. M. Khater, et al., Solution of fractional-order Korteweg-de Vries and Burgers' equations utilizing local meshless method, *J. Ocean Eng. Sci.*, 2021. https://doi.org/10.1016/j.joes.2021.08.014
6. I. Ahmad, I. Ali, R. Jan, S. A. Idris, M. Mousa, Solutions of a three-dimensional multi-term fractional anomalous solute transport model for contamination in groundwater, *Plos One*, **18** (2023), e0294348. https://doi.org/10.1371/journal.pone.0294348
7. F. Wang, M. N. Khan, I. Ahmad, H. Ahmad, H. Abu-Zinadah, Y. M. Chu, Numerical solution of traveling waves in chemical kinetics: time-fractional Fishers equations, *Fractals*, **30** (2022), 2240051. https://doi.org/10.1142/S0218348X22400515
8. H. Ahmad, T. A. Khan, I. Ahmad, P. S. Stanimirović, Y. M. Chu, A new analyzing technique for nonlinear time fractional Cauchy reaction-diffusion model equations, *Results Phys.*, **19** (2020), 103462. https://doi.org/10.1016/j.rinp.2020.103462
9. M. Inc, M. N. Khan, I. Ahmad, S. W. Yao, H. Ahmad, P. Thounthong, Analysing time-fractional exotic options via efficient local meshless method, *Results Phys.*, **19** (2020), 103385. https://doi.org/10.1016/j.rinp.2020.103385
10. H. Ahmad, M. N. Khan, I. Ahmad, M. Omri, M. F. Alotaibi, A meshless method for numerical solutions of linear and nonlinear time-fractional Black-Scholes models. *AIMS Math.*, **8** (2023), 19677–19698. https://doi.org/10.3934/math.20231003
11. B. Almutairi, I. Ahmad, B. Almohsen, H. Ahmad, D. U. Ozsahin, Numerical simulations of time-fractional PDEs arising in mathematics and physics using the local meshless differential quadrature method, *Therm. Sci.*, **27** (2023), 263–272. https://doi.org/10.2298/TSCI23S1263A
12. H. Irshad, M. Shakeel, I. Ahmad, H. Ahmad, C. Tearnbucha, W. Sudsutad, Simulation of generalized time fractional Gardner equation utilizing in plasma physics for non-linear propagation of ion-acoustic waves, *Therm. Sci.*, **27** (2023), 121–128. https://doi.org/10.2298/TSCI23S1121I
13. I. Ahmad, A. R. Seadawy, H. Ahmad, P. Thounthong, F. Wang, Numerical study of multi-dimensional hyperbolic telegraph equations arising in nuclear material science via an efficient local meshless method, *Int. J. Nonlinear Sci. Numer.*, **23** (2022), 115–122. https://doi.org/10.1515/ijnsns-2020-0166
14. Z. Hussain, S. Khan, A. Ullah, Ikramullah, M. Ayaz, I. Ahmad, et al., Extension of optimal homotopy asymptotic method with use of Daftardar-Jeffery polynomials to Hirota-Satsuma coupled system of Korteweg-de Vries equations, *Open Phys.*, **18** (2020), 916–924. https://doi.org/10.1515/phys-2020-0210
15. F. Wang, J. Zhang, I. Ahmad, A. Farooq, H. Ahmad, A novel meshfree strategy for a viscous wave equation with variable coefficients, *Front Phys.*, **9** (2021), 701512. https://doi.org/10.3389/fphy.2021.701512
16. M. Ahsan, A. A. Khan, S. Dinibutun, I. Ahmad, H. Ahmad, N. Jarasthitikulchai, et al., The haar wavelets based numerical solution of Reccati equation with integral boundary condition, *Therm. Sci.*, **27** (2023), 93–100. https://doi.org/10.2298/TSCI23S1093A
17. K. Srinivasa, R. A. Mundewadi, Wavelets approach for the solution of nonlinear variable delay differential equations, *Int. J. Math. Comput. Eng.*, **1** (2023), 139–148. https://doi.org/10.2478/ijmce-2023-0011
18. R. Singh, J. Mishra, V. K. Gupta, The dynamical analysis of a Tumor Growth model under the effect of fractal fractional Caputo-Fabrizio derivative, *Int. J. Math. Compt. Eng.*, **1** (2023), 115–126. https://doi.org/10.2478/ijmce-2023-0009
19. F. Wang, I. Ahmad, H. Ahmad, H. Ahmad, K. S. Alimgeer, C. Cesarano, et al., Meshless method based on RBFs for solving three-dimensional multi-term time fractional PDEs arising in engineering phenomenons, *J. King Saud Univ. Sci.*, **33** (2021), 101604. https://doi.org/10.1016/j.jksus.2021.101604

20. A. H. Arnous, M. S. Hashemi, K. S. Nisar, M. Shakeel, J. Ahmad, I. Ahmad, et al., Investigating solitary wave solutions with enhanced algebraic method for new extended Sakovich equations in fluid dynamics, *Results Phys.*, **57** (2024), 107369. https://doi.org/10.1016/j.rinp.2024.107369

21. V. G. Drinfel'd, V. V. Sokolov, Lie algebras and equations of Korteweg-de Vries type, *J. Soviet Math.*, **30** (1985), 1975–2036. https://doi.org/10.1007/BF02105860

22. G. Wilson, The affine Lie algebra $C_2^{(1)}$ and an equation of Hirota and Satsuma, *Phys. Lett. A*, **89** (1982), 332–334. https://doi.org/10.1016/0375-9601(82)90186-4

23. Z. X. Qin, Z. H. Yan, An improved F-expansion method and its application to coupled Drinfeld-Sokolov-Wilson equation, *Commun. Theor. Phys.*, **50** (2008), 309. https://doi.org/10.1088/0253-6102/50/2/05

24. R. Arora, A. Kumar, Solution of the coupled Drinfeld's-Sokolov-Wilson (DSW) system by homotopy analysis method, *Adv. Sci. Eng. Med.*, **5** (2013), 1105–1111. https://doi.org/10.1166/asem.2013.1399

25. W. Liu, Y. Zhang, Time-fractional Drinfeld-Sokolov-Wilson system: Lie symmetry analysis, analytical solutions and conservation laws, *Eur. Phys. J. Plus*, **134** (2019), 126. https://doi.org/10.1140/epjp/i2019-12490-8

26. M. Inc, On numerical doubly periodic wave solutions of the coupled Drinfel'd-Sokolov-Wilson equation by the decomposition method, *Appl. Math. Comput.*, **172** (2006), 421–430. https://doi.org/10.1016/j.amc.2005.02.012

27. R. Islam, K. Khan, M. A. Akbar, M. E. Islam, M. T. Ahmed, Traveling wave solutions of some nonlinear evolution equations, *Alex. Eng. J.*, **54** (2015), 263–269. https://doi.org/10.1016/j.aej.2015.01.002

28. J. Moser, *Dynamical systems, theory and applications*, Springer, 1975. https://doi.org/10.1007/3-540-07171-7

29. V. Dougalis, F. Sturm, G. Zouraris, On an initial-boundary value problem for a wide-angle parabolic equation in a waveguide with a variable bottom, *Math. Methods Appl. Sci.*, **32** (2009), 1519–1540. https://doi.org/10.1002/mma.1097

30. S. Kumar, M. P. Tripathi, O. P. Singh, A fractional model of Harry Dym equation and its approximate solution, *Ain Shams Eng. J.*, **4** (2013), 111–115. https://doi.org/10.1016/j.asej.2012.07.001

31. I. Ahmad, M. Ahsan, I. Hussain, P. Kumam, W. Kumam, Numerical simulation of PDEs by local meshless differential quadrature collocation method, *Symmetry*, **11** (2019), 394. https://doi.org/10.3390/sym11030394

32. P. Thounthong, M. N. Khan, I. Hussain, I. Ahmad, P. Kumam, Symmetric radial basis function method for simulation of elliptic partial differential equations, *Mathematics*, **6** (2018), 327. https://doi.org/10.3390/math6120327

33. I. Ahmad, M. Riaz, M. Ayaz, M. Arif, S. Islam, P. Kumam, Numerical simulation of partial differential equations via local meshless method, *Symmetry*, **11** (2019), 257. https://doi.org/10.3390/sym11020257

34. M. Nawaz, I. Ahmad, H. Ahmad, A radial basis function collocation method for space-dependent inverse heat problems, *J. Appl. Comput. Mech.*, **6** (2020), 1187–1199. https://doi.org/10.22055/JACM.2020.32999.2123

35. I. Ahmad, S. ul Islam, A. Q. M. Khaliq, Local RBF method for multi-dimensional partial differential equations, *Comput. Math. Appl.*, **74** (2017), 292–324. https://doi.org/10.1016/j.camwa.2017.04.026

36. I. Ahmad, H Ahmad, P. Thounthong, Y. M. Chu, C. Cesarano, Solution of multi-term time-fractional PDE models arising in mathematical biology and physics by local meshless method, *Symmetry*, **12** (2020), 1195. https://doi.org/10.3390/sym12071195

37. M. I. Bhatti, M. H. Rahman, N. Dimakis, Approximate solutions of nonlinear partial differential equations using B-polynomial bases, *Fractal Fract.*, **5** (2021), 106. https://doi.org/10.3390/fractalfract5030106

38. A. Davari, A. Ahmadi, New implementation of legendre polynomials for solving partial differential equations, *Appl. Math.*, **4** (2013), 1647. https://doi.org/10.4236/am.2013.412224

39. I. Ahmad, A. A. Bakar, I. Ali, S. Haq, S. Yussof, A. H. Ali, Computational analysis of time-fractional models in energy infrastructure applications. *Alex. Eng. J.*, **82** (2023), 426–436. https://doi.org/10.1016/j.aej.2023.09.057

40. N. N. H. Shah, R. Jan, H. Ahmad, N. N. A. Razak, I. Ahmad, H. Ahmad, Enhancing public health strategies for tungiasis: A mathematical approach with fractional derivative, *AIMS Bioeng.*, **10** (2023), 384–405. https://doi.org/10.3934/bioeng.2023023

41. G. Jumarie, Stock exchange fractional dynamics defined as fractional exponential growth driven by (usual) Gaussian white noise. Application to fractional Black-Scholes equations, *Insur. Math. Econ.*, **42** (2008), 271–287. https://doi.org/10.1016/j.insmatheco.2007.03.001

42. G. Jumarie, Derivation and solutions of some fractional Black-Scholes equations in coarse-grained space and time, Application to Merton's optimal portfolio, *Comput. Math. Appl.*, **59** (2010), 1142–1164. https://doi.org/10.1016/j.camwa.2009.05.015

43. M. Caputo, Linear models of dissipation whose Q is almost frequency independent-II, *Geophys. J. Int.*, **13** (1967), 529–539. https://doi.org/10.1111/j.1365-246X.1967.tb02303.x

44. A. Atangana, D. Baleanu, New fractional derivatives with non-local and nonsingular kernel theory and application to heat transfer model, *Therm. Sci*, **20** (2016), 763–769. https://doi.org/10.2298/TSCI160111018A

45. J. He, Z. Li, Q. Wang, A new fractional derivative and its application to explanation of polar bear hairs, *J. King Saud. Univ. Sci.*, **28** (2016), 190–192. https://doi.org/10.1016/j.jksus.2015.03.004

46. Z. Sun, X. Wu, A fully discrete difference scheme for a diffusion-wave system, *Appl. Numer. Math.*, **56** (2006), 193–209. https://doi.org/10.1016/j.apnum.2005.03.003

47. G. E. Fasshauer, *Meshfree approximation methods with MATLAB*, World Scientific, 2007.

48. H. Wendland, Local polynomial reproduction and moving least squares approximation, *IMA J. Numer. Anal.*, **21** (2001), 285–300. https://doi.org/10.1093/imanum/21.1.285

49. P. D. Lax, Weak solutions of nonlinear hyperbolic equations and their numerical computation, *Commun. Pure Appl. Math.*, **7** (1954), 159–193. https://doi.org/10.1002/cpa.3160070112

50. R. Mokhtari, Exact solutions of the Harry-Dym equation, *Commun. Theor. Phys.*, **55** (2011), 204. https://doi.org/10.1088/0253-6102/55/2/03

51. A. Ghafoor, S. Sardar, A. Ullah, M. Hussain, H. Ahmad, F. A. Awwad, et al., Simulations of the one and two dimensional nonlinear evolutionary partial differential equations: a numerical study, *Results Phys.*, **49** (2023), 106466. https://doi.org/10.1016/j.rinp.2023.106466

52. M. Rawashdeh, A new approach to solve the fractional Harry Dym equation using the FRDTM, *Int. J. Pure Appl. Math.*, **95** (2014), 553–566. https://doi.org/10.12732/ijpam.v95i4.8

AIMS Press